

# Singular boundary method using time-dependent fundamental solution for scalar wave equations

Wen Chen<sup>1,2</sup> · Junpu Li<sup>1,2</sup> · Zhuojia Fu<sup>1,2</sup>

Received: 2 February 2016 / Accepted: 2 July 2016 / Published online: 14 July 2016  
© Springer-Verlag Berlin Heidelberg 2016

**Abstract** This study makes the first attempt to extend the meshless boundary-discretization singular boundary method (SBM) with time-dependent fundamental solution to two-dimensional and three-dimensional scalar wave equation upon Dirichlet boundary condition. The two empirical formulas are also proposed to determine the source intensity factors. In 2D problems, the fundamental solution integrating along with time is applied. In 3D problems, a time-successive evaluation approach without complicated mathematical transform is proposed. Numerical investigations show that the present SBM methodology produces the accurate results for 2D and 3D time-dependent wave problems with varied velocities  $c$  and wave numbers  $k$ .

**Keywords** Singular boundary method · Time-dependent fundamental solutions · Wave equation · Empirical formulas · Boundary discretization method

## 1 Introduction

The phenomenon of wave propagation is widely encountered in a variety of engineering disciplines, such as the stress wave in an elastic solid, water wave, and sound wave etc [1–3]. The development of highly accurate and efficient wave

solvers remains an important and challenging research topic even though there are diverse numerical methods available today for solving the wave equation, such as the finite element method (FEM) [4–6], the boundary element method (BEM) [7–9], the method of fundamental solutions (MFS) [10–12] the finite difference method [13, 14], the finite volume method [15, 16], and, most recently, meshless method [17–19].

However, the standard domain discretization methods such as the finite element, finite difference and finite volume methods, require troublesome mesh generation for 3D problems and are not efficient for unbounded domain problems. On the other hand, the BEM encounters time-consuming and mathematically sophisticated issue of the numerical integration over singularities. As for the MFS, the placement of the fictitious boundary is vital for its reliability and numerical accuracy, and remains an open issue to be optimally determined, especially for multi-connected or complex-shaped domain problems.

To remedy the above-mentioned drawbacks, the SBM [20] was proposed in 2009 as a strong-form boundary collocation method free of mesh and integration. In order to regularize the singularities of the fundamental solutions upon the coincidence of the source and collocation points, the concept of the source intensity factors (SIFs) was introduced, and it is also called the origin intensity factors in some literatures [20]. The SBM overcomes the harassing mesh generation in the traditional FEM and the perplexing fictitious boundary in the MFS. On the other hand, in comparison with the BEM [21–23], the SBM introduces the SIFs to instead of singular integrals, which makes the SBM get higher numerical accuracy and faster convergence rate than the BEM with the same computing resources [24].

Under the extensive studies, several techniques have been proposed to determine the SIFs in the SBM of both the fun-

✉ Wen Chen  
chenwen@hhu.edu.cn

<sup>1</sup> State Key Laboratory of Hydrology-Water Resources and Hydraulic Engineering & Center for Numerical Simulation Software in Engineering and Sciences, College of Mechanics and Materials, Hohai University, Nanjing 210098, Jiangsu, China

<sup>2</sup> State Key Laboratory of Acoustics, Institute of Acoustics, Chinese Academy of Sciences, Beijing 100190, China

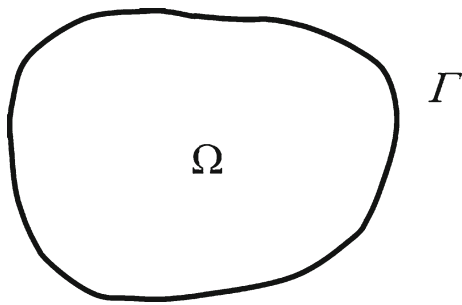


**Fig. 1** Domain of the 2D scalar wave equation

damental solutions and their derivatives [25, 26]. Numerical investigations show that these techniques help the SBM provide accurate solutions in the Helmholtz [27], potential [20], water wave [28, 29], elastic and acoustic waves [30] problems with arbitrarily complex-shaped computational geometries.

This study makes the first attempt to extend the SBM with time-dependent fundamental solution to 2D and 3D scalar wave equations upon Dirichlet boundary condition. In the present SBM formulation, two empirical formulas are proposed to determine the SIFs. In 2D problems, the fundamental solution integrating along with time is applied. In 3D problems, a time-successive evaluation approach without complicated mathematical transform is proposed. A brief outline of this paper is as follows. Section 2 describes the numerical methodology of the SBM using time-dependent fundamental solution for scalar wave equations. In Sect. 3, the efficiency and accuracy of the present approach are examined in 2D and 3D benchmark examples in comparison with the analytical and linear BEM solutions. Finally, Sect. 4 concludes this study with some remarks.

## 2 Numerical methodology

### 2.1 SBM for 2D wave equation with Dirichlet boundary condition

The 2D time-dependent wave equation can be written as

$$u = \begin{cases} \Delta u - \frac{1}{c^2} \frac{\partial^2 u}{\partial t^2} = 0, & (x, y) \in \Omega, \quad t > 0 \\ u|_{\Gamma} = \bar{u} \\ u|_{t=0} = u_0, \quad \frac{\partial u}{\partial t}|_{t=0} = v_1 \end{cases}, \quad (1)$$

where  $\Omega$  is the computational domain with boundary  $\Gamma$  as shown in Fig. 1,  $u$  the physical variable,  $c$  the wave speed,  $t$  denotes time.

The fundamental solution of 2D scalar wave equation is given by

$$G(t, r) = \frac{c}{2\pi\sqrt{c^2t^2 - r^2}} H(ct - r), \quad (2)$$

where the  $H(x)$  is the Heaviside function

$$H(x) = \begin{cases} 0 & \text{for } x < 0 \\ 1/2 & \text{for } x = 0 \\ 1 & \text{for } x > 0 \end{cases}. \quad (3)$$

The original wave equation  $u$  can be interpreted as an initial-boundary value problems. In this paper, basing on the superposition principle, we split the original equation into two parts, i.e.,  $u_1$  and  $u_2$ .  $u_1$  can be interpreted as a boundary value problem and  $u_2$  can be considered the initial value problem. The solution of Eq. (1) can be separated as  $u = u_1^* + u_2^*$ , where

$$u_1^* = \begin{cases} \Delta u_1^* - \frac{1}{c^2} \frac{\partial^2 u_1^*}{\partial t^2} = 0, & (x, y) \in \Omega, \quad t > 0 \\ u_1^*|_{\Gamma} = \bar{u} - \bar{u}_2^* = \bar{u}_1^* \\ u_1^*|_{t=0} = 0, \quad \frac{\partial u_1^*}{\partial t}|_{t=0} = 0 \end{cases}, \quad (4)$$

$$u_2^* = \begin{cases} \Delta u_2^* - \frac{1}{c^2} \frac{\partial^2 u_2^*}{\partial t^2} = 0, & t > 0 \\ u_2^*|_{\Gamma} = \bar{u}_2^* \\ u_2^*|_{t=0} = 0, \quad \frac{\partial u_2^*}{\partial t}|_{t=0} = 0 & (x, y) \notin \Omega \\ u_2^*|_{t=0} = u_0, \quad \frac{\partial u_2^*}{\partial t}|_{t=0} = v_1 & (x, y) \in \Omega \end{cases}. \quad (5)$$

At first, consider the initial value problem Eq. (5), the  $u_2^*$  can be calculated directly by using 2D poisson formulation [17]

$$u_2^*(x_i, t_n) = \frac{1}{c^2} \iint_{C_{ct_n}^{M_0}} u_0 \frac{\partial G}{\partial n} ds + \frac{1}{c^2} \iint_{C_{ct_n}^{M_0}} v_1 G ds, \quad x_i \in \Omega, \quad t_n > 0. \quad (6)$$

where  $u_2^*(x_i, t_n)$  represents the physical variable  $u_2^*$  for the point  $x_i$  in domain  $\Omega$  at time level  $t_n$ s,  $C_{ct_n}^{M_0}$  the circular domain with radius  $ct_n$ ,  $M_0$  the projection point of the computation point  $M$ , at the  $t = 0$ s plane in the domain  $\Omega$ , and the center point of the circular domain  $C_{ct_n}^{M_0}$ . In Eq. (5), we only need to calculate Eq. (6) in  $C_{ct_n}^{M_0} \cap \Omega$  domain, called the corresponding range of influence of the computation point  $M$  in this paper. And then the SBM only places the field points in  $C_{ct_n}^{M_0} \cap \Omega$  domain for every computation point  $M$  as shown in Fig. 2a, b.

In the 2D poisson formulation, the fundamental solution  $G$  have singularities when  $r = ct \neq 0$ . To remove these singularities, we introduce a non-singular integral approach. This paper replaces the point source by using line source from  $r_1$  to  $r_2$  at arbitrary angles as shown in Fig. 3.

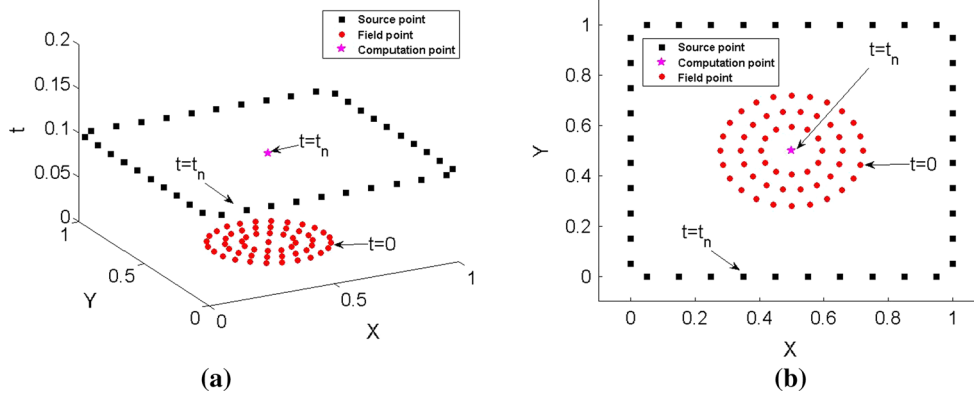


Fig. 2 Distribution of the source, field and computation points a 3D plot; b 2D contour plot

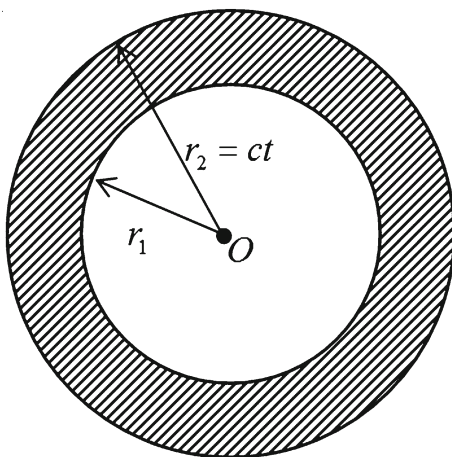


Fig. 3 Domain of the annulus

The singular term  $G_{ii}$  can be represented as follows

$$G_{ii} = \frac{\int_{r_1}^{r_2} \frac{cr}{\sqrt{c^2t^2 - r^2}} dr}{\pi(r_2^2 - r_1^2)} \quad \text{when } r = ct \neq 0. \quad (7)$$

Then it can be rewritten as

$$G_{ii} = \frac{c}{\pi\sqrt{r_2^2 - r_1^2}} \quad \text{when } r = ct \neq 0, \quad (8)$$

where point  $O$  is at  $(0, 0, t)$ ,  $r_2 = ct$  denotes the outer radius,  $r_1$  represents the inner radius. And the annulus domain is on  $t = 0s$  plane.

Then, consider the boundary value problem Eq. (4). The SBM uses the fundamental solution  $G$  integrating along with time as the kernel function

$$G^* = \int_0^t G d\tau = \frac{1}{2\pi} \left[ H(c(t - \tau) - r) \cosh^{-1}(c(t - \tau)/r) \right] \Big|_{\tau=0}^{\tau=t}, \quad (9)$$

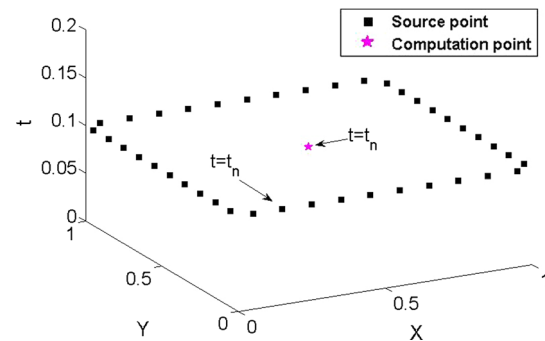


Fig. 4 Distribution of the source points

where  $G^*$  is the fundamental solution  $G$  integrating along with time, i.e.,  $G^* = \int_0^t G d\tau$ .

When we need to calculate the physical variable  $u_1^*$  in domain  $\Omega$  at  $t_n s$ , the SBM only places the source points on the physical boundary  $\Gamma$  at  $t = t_n s$  as shown in Fig. 4. The solution  $u_1^*(x_i, t_n)$  for the computation point  $x_i$  in domain  $\Omega$  at  $t = t_n s$  can be approximated by a linear combination of kernel function  $G^*$  with respect to different source points  $s_j$  as below

$$u_1^*(x_i, t_n) = u(x_i, t_n) - u_2^*(x_i, t_n) = \sum_{j=1}^N \alpha_j(t_n) G^*(|x_i - s_j|, t_n), \quad (10)$$

where  $u_1^*(x_i, t_n)$  represents the physical variable  $u_1^*$  of the point  $x_i$  in domain  $\Omega$  at time level  $t_n s$ ,  $N$  the number of source points,  $\alpha_j(t_n)$  the  $j$ th unknown coefficient at time level  $t_n s$ ,  $G^*(|x_i - s_j|, t_n) = \int_0^{t_n} G d\tau$  the kernel function at  $t_n s$ ,  $|x_i - s_j|$  the distance between source point  $s_j$  and collocation point  $x_i$ .

The SBM places all computing nodes on the same physical boundary. Consequently, the source points  $\{s_j\}$  and the collocation points  $\{x_i\}$  are the same set of boundary nodes. The kernel function  $G^*$  encounters singularities when  $x_i = s_j$ .

To solve this singular problem, the SBM introduces the concept of the source intensity factors. When  $x_i = s_j$ , we use source intensity factors replacing the singular terms in the SBM interpolation formulation. Thus the SBM interpolation formulation can be expressed as

$$\begin{aligned} \bar{u}_1^*(x_i, t_n) &= \bar{u}(x_i, t_n) - \bar{u}_2^*(x_i, t_n) \\ &= \sum_{j=1, j \neq i}^N \alpha_j(t_n) G^*(|x_i - s_j|, t_n) \\ &\quad + \alpha_i Q_i^*(t_n), \end{aligned} \tag{11}$$

where  $\bar{u}_1^*(x_i, t_n)$  is the solution of the Eq. (4) for the collocation point  $x_i$  on the boundary  $\Gamma$  at  $t_n s$ ,  $\bar{u}_2^*(x_i, t_n)$  the solution of the Eq. (5) for the collocation point  $x_i$  on the boundary  $\Gamma$  at  $t_n s$  and  $\bar{u}(x_i, t_n)$  the solution of the Eq. (1) for the collocation point  $x_i$  on the boundary  $\Gamma$  at  $t_n s$ .  $Q_i^*(t_n)$  denotes the SIFs at  $t_n s$ . The technique to determine the SIFs will be introduced in the subsequent section. By substituting the boundary conditions  $\bar{u}(x_i, t_n)$ ,  $\bar{u}_2^*(x_i, t_n)$  and source intensity factors  $Q_i^*(t_n)$  into Eq. (11), we can determine the unknown coefficients  $\{\alpha_j(t_n)\}$  from Eq. (11). After we get the unknown coefficients  $\{\alpha_j(t_n)\}$ , the solution  $u_1^*(x_i, t_n)$  of Eq. (4) in the computational domain  $\Omega$  at  $t_n s$  can be obtained from Eq. (10).

With the superposition principle, the solution  $u(x_i, t_n)$  of Eq. (1) in the computational domain  $\Omega$  at time level  $t_n s$  can be obtained from  $u = u_1^* + u_2^*$ . Fig. 2a, b illustrate the location of the source and the field points for one computation point  $M$  in domain  $\Omega$ .

The technique to determine the SIFs will be introduced in this section. In comparison with the inverse interpolation technique (IIT) [30], an empirical formula is proposed to determine the SIFs of the kernel function  $G^*$  at  $x_i = s_j$  in Eq. (11). The kernel function  $G^*$  can also be written as

$$\begin{aligned} G^* &= \int_0^t G d\tau = \frac{1}{2\pi} \left[ H(c(t - \tau) - r) (\log(c(t - \tau) \right. \\ &\quad \left. + \sqrt{c^2(t - \tau)^2 - r^2}) - \log(r)) \right] \Big|_{\tau=0}^{\tau=t}. \end{aligned} \tag{12}$$

It can be found that the kernel function  $G^*$  has the same order of singularities with the fundamental solution of 2D Laplace equation  $\log(r)$  when  $s_i = s_j$  [30]. By implementing the SIF empirical formula of 2D Laplace equation [25]

$$G_0^j = \log\left(\frac{L_j}{2\pi}\right). \tag{13}$$

The detailed derivation of Eq. (13) is given in Appendix 1. The SIFs at time level  $t_n$  of 2D wave equation can be given by

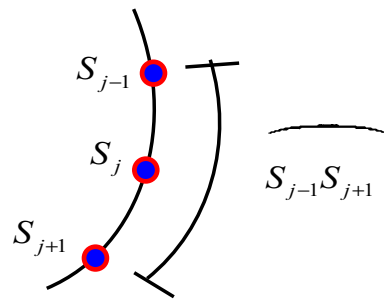


Fig. 5 The schematic configuration of the source points  $s_j$  and the curve  $s_{j-1}s_{j+1}$  in 2D problems

$$\begin{aligned} Q_j^*(t_n) &= \frac{1}{2\pi} \left[ H(c(t_n - \tau) - \frac{L_j}{2\pi}) (\log(c(t_n - \tau) \right. \\ &\quad \left. + \sqrt{c^2(t_n - \tau)^2 - (\frac{L_j}{2\pi})^2}) - \log(\frac{L_j}{2\pi})) \right] \Big|_{\tau=0}^{\tau=t_n}, \end{aligned} \tag{14}$$

where  $L_j$  is the corresponding range of influence of the source point  $s_j$ . For 2D problem,  $L_j$  is half length of the curve  $s_{j-1}s_{j+1}$  between the source points  $s_{j-1}$  and  $s_{j+1}$  as shown in Fig. 5.

To investigate the accuracy and efficiency of the proposed empirical formulas, we make the investigation on numerical accuracy of the empirical formula against time  $t$  as shown in Fig. 6. The X axis is

$$\log\left(c(t - \tau) + \sqrt{c^2(t - \tau)^2 - \left(\frac{L_j}{2\pi}\right)^2}\right) \tag{15}$$

And the Y axis is the source intensity factors.

We find that the slope of the linear fitting curve is about  $0.1592 \approx \frac{1}{2\pi}$ , which is in good agreement with Eq. (14). It can be demonstrated that the form of the present empirical formula is valid in time direction.

Then, Fig. 7 shows the SIFs obtained by the empirical formula (14) and the inverse interpolation technique against the corresponding influence area  $L_j$ , and the test domain is a circle with radius 1. It can be observed that the SIFs obtained by the empirical formula are in good agreement with the inverse interpolation technique results with  $Err = 2.61E - 3$ .

And it is worthy of stressing that there is still no analytical solution of the SIFs for 2D wave problems. By using the inverse interpolation technique, the SIFs can easily be calculated, but the inverse interpolation technique is not always numerically stable because of the inverse interpolation, and this is also the reason that we do the present study to find an empirical formula to evaluate the SIFs. In this paper, the

**Fig. 6** The source intensity factors against time

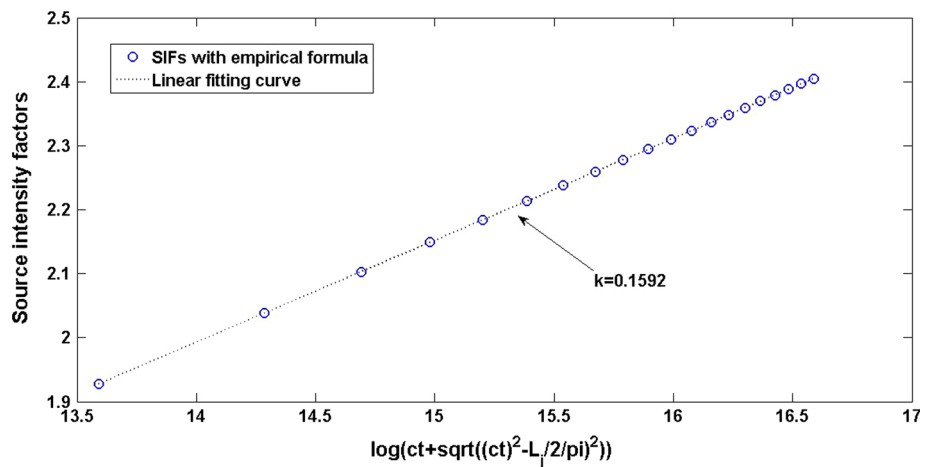
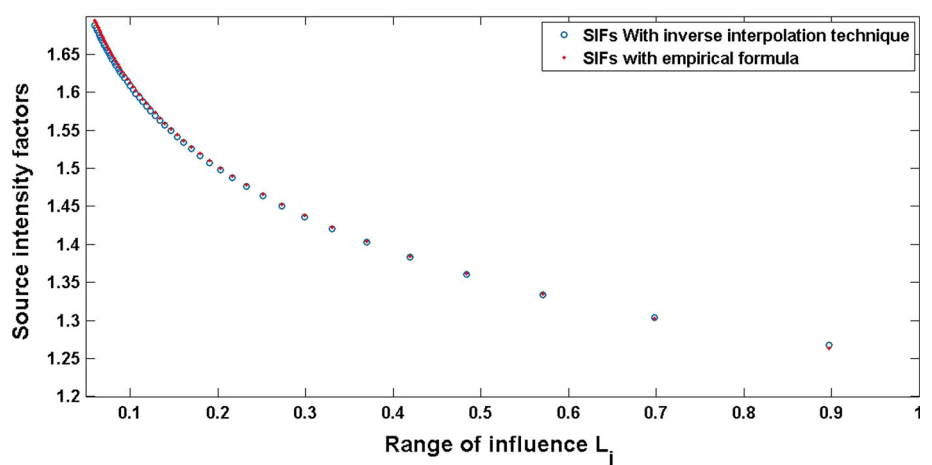


**Fig. 7** The source intensity factors against the range of influence  $L_j$



SIFs with the inverse interpolation technique is used as a reference solution (blue circle in Fig. 7) to verify the accuracy and efficiency of the proposed empirical formula (red point in Fig. 7).

**2.2 SBM for 3D wave equation with Dirichlet boundary condition**

The 3D time-dependent wave equation is stated as

$$u = \begin{cases} \Delta u - \frac{1}{c^2} \frac{\partial^2 u}{\partial t^2} = 0, & (x, y, z) \in \Omega, \quad t > 0 \\ u|_{\Gamma} = \bar{u} \\ u|_{t=0} = u_0, \quad \frac{\partial u}{\partial t}|_{t=0} = v_1 \end{cases} \quad (16)$$

Its fundamental solutions is

$$G(r, t) = \frac{1}{4\pi r} \delta[(t - \tau) - r/c], \quad (17)$$

where  $\delta$  is the Dirac delta distribution. Note that the fundamental solution  $G$  merely expresses the present potential in values of the potential at previous moments called the

retarded moment. The retardation corresponds to the time required for a wave to travel between the source and the collocation points. Consequently, once the corresponding unknown coefficients  $\{\alpha_j(t_R)\}$  of the source points  $\{s_j\}$  are obtained at a certain time, the numerical results at the next time step can be calculated.

By analogy with the SBM for 2D wave equation, the solution of Eq. (16) can be split as  $u = u_1^* + u_2^*$ .

$$u_1^* = \begin{cases} \Delta u_1^* - \frac{1}{c^2} \frac{\partial^2 u_1^*}{\partial t^2} = 0, & (x, y, z) \in \Omega, \quad t > 0 \\ u_1^*|_{\Gamma} = \bar{u} - \bar{u}_2^* = \bar{u}_1^* \\ u_1^*|_{t=0} = 0, \quad \frac{\partial u_1^*}{\partial t}|_{t=0} = 0 \end{cases} \quad (18)$$

$$u_2^* = \begin{cases} \Delta u_2^* - \frac{1}{c^2} \frac{\partial^2 u_2^*}{\partial t^2} = 0, & t > 0 \\ u_2^*|_{\Gamma} = \bar{u}_2^* \\ u_2^*|_{t=0} = 0, \quad \frac{\partial u_2^*}{\partial t}|_{t=0} = 0 & (x, y, z) \notin \Omega \\ u_2^*|_{t=0} = u_0, \quad \frac{\partial u_2^*}{\partial t}|_{t=0} = v_1 & (x, y, z) \in \Omega \end{cases} \quad (19)$$

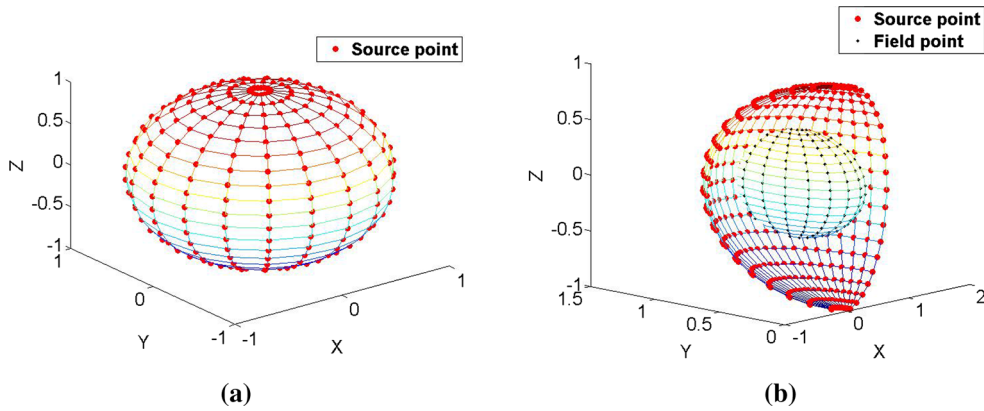


**Fig. 8** The Distribution of the source and the field points for 3D problems

The solution  $u_2^*$  of Eq. (19) can be calculated directly by using the following 3D poisson formulation [18]

$$u_2^*(x_i, t_n) = \frac{1}{4\pi} \frac{\partial}{\partial r} \iint_{S_{ct_n}^M} \frac{u_0}{r} ds + \frac{1}{4c\pi} \iint_{S_{ct_n}^M} \frac{v_1}{r} ds, \quad x_i \in \Omega, \tag{20}$$

where  $u_2^*(x_i, t_n)$  represents the physical variable  $u_2^*$  of the point  $x_i$  in domain  $\Omega$  at time level  $t_n$ .  $S_{ct_n}^M$  is a sphere surface with radius  $ct_n$ ,  $M$  the center point of the sphere surface. In Eq. (19), we only need to calculate Eq. (20) in  $S_{ct_n}^M \cap \Omega$  domain, called the corresponding range of influence of the computation point  $M$  in this paper. So the SBM only places field points in the  $S_{ct_n}^M \cap \Omega$  domain for every computation point  $M$  as shown in Fig. 8b.

Then, consider the solution  $u_1^*$  of Eq. (18), with the Huygens principle, “every point on the boundary reached by a wave acts as a source” [18]. We can assume that there is a series of wave sources  $\alpha(r) = \gamma(x_m, \bar{u}, t)$  on the boundary, the sum of these secondary waves determines the form of the wave at any subsequent time in the domain  $\Omega$ . Where  $\alpha(r) = \gamma(x_m, \bar{u}, t)$  denotes the secondary wave source intensity. Then, the physical variable  $u_1^*(x_i, t_n)$  in the domain  $\Omega$  at time level  $t_n$  can be expressed as

$$u_1^*(x_i, t_n) = \iiint_{\Omega} \frac{\alpha(r)}{4\pi r} \delta\left(t_n - \frac{r}{c}\right) dv, \quad x_i \in \Omega, \quad t_n > 0. \tag{21}$$

The SBM places the source points on the boundary  $\Gamma$  as shown in Fig. 8a, and uses  $\Delta t$  as the time interval. The superscripts of  $t$  represent the time level. The solution  $u_1^*(x_i, t_n)$  for the computation point  $x_i$  in domain  $\Omega$  at  $t_n \in ((n - 1) \Delta t, n \Delta t)$  can be approximated by a linear combination of fundamental solution  $G$  with respect to different source points  $s_j$  as below

$$u_1^*(x_i, t_n) = u(x_i, t_n) - u_2^*(x_i, t_n) = \sum_{j=1}^N \alpha_j(t_R) G(|x_i - s_j|, t_R), \tag{22}$$

$$t_R = t_n - \frac{r}{c} > 0 \quad i = 1, 2, 3, \dots$$

where  $\alpha_j(t_R)$  is the  $j$ th unknown coefficient at the retarded moment  $t_R$ ,  $G(|x_i - s_j|, t_R)$  the fundamental solution of 3D scalar wave equation at the retarded moment  $t_R$ ,  $|x_i - s_j|$  the distance between source point  $s_j$  and collocation point  $x_i$ .

In time-harmonic wave, we can assume that

$$\alpha_j(t_R) = \alpha_j^*(t_R) e^{-i\omega t_R} \approx \alpha_j^*(t_m \Delta t) e^{-i\omega t_R}, \tag{23}$$

where  $0 \leq t_m \Delta t - t_R < \Delta t$ , if  $t_R < 0$ , the wave does not reach the collocation points,  $\alpha_j(t_R) = \alpha_j^*(t_R) = 0$ .  $\omega$  denotes the wave frequency,  $k = \omega/c$  the wave number.

When  $x_i = s_j$ , we use source intensity factors replacing the singular terms in the SBM interpolation formulation. The technique to determine the SIFs will be introduced in the subsequent section. Thus, the SBM interpolation formulation can be expressed as

$$\bar{u}_1^*(x_i, t_n) = \bar{u}(x_i, t_n) - \bar{u}_2^*(x_i, t_n) = \sum_{j=1, j \neq i}^N \alpha_j(t_R) G(|x_i - s_j|, t_R) + \alpha_i(t_R) Q_i(t_R), \tag{24}$$

$$t_R = t_n - \frac{r}{c} > 0 \quad i = 1, 2, 3, \dots$$

$$\alpha_j(t_R) = \alpha_j^*(t_R) e^{-i\omega t_R} \approx \alpha_j^*(t_m \Delta t) e^{-i\omega t_R}, \tag{25}$$

where  $\bar{u}_1^*(x_i, t_n)$  is the solution of the Eq. (18) for the collocation point  $x_i$  on the boundary  $\Gamma$  at  $t_n$ ,  $\bar{u}_2^*(x_i, t_n)$  the solution of the Eq. (19) for the collocation point  $x_i$  on the boundary  $\Gamma$  at  $t_n$  and  $\bar{u}(x_i, t_n)$  the solution of the Eq. (16) for the collocation point  $x_i$  on the boundary  $\Gamma$  at  $t_n$ .  $Q_i(t_R)$  the SIFs



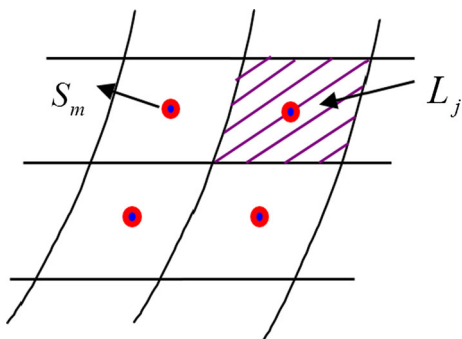


**Fig. 9** The source points  $s_j$  and the corresponding infinitesimal area  $L_j$  in 3D problems

at the retarded moment,  $0 \leq t_{m\Delta t} - t_R < \Delta t$ , if  $m < n$ , the unknown coefficient  $\alpha_j(t_R)$  has been calculated in the previous steps. If  $t_R < 0$ , the wave does not reach the collocation points,  $\alpha_j(t_R) = \alpha_j^*(t_R) = 0$ .  $\omega$  denotes the wave frequency,  $k = \omega/c$  the wave number. By substituting the boundary conditions  $\bar{u}(x_i, t_n)$ ,  $\bar{u}_2^*(x_i, t_n)$  and source intensity factors  $Q_i(t_R)$  into Eqs. (24) and (25), we can calculate the unknown coefficient  $\alpha_j^*(t_{n\Delta t})$  at  $t_n = n\Delta t$  and  $\alpha_j(t_R)$  at the retarded moment. At last, the solutions  $u_1^*(x_i, t_n)$  of the Eq. (18) in the computational domain  $\Omega$  at  $t_{ns}$  can be obtained from Eqs. (22) and (23).

With the superposition principle, the solution  $u(x_i, t_n)$  of Eq. (16) for the computation point  $x_i$  in the computational domain  $\Omega$  at time level  $t_{ns}$  can be obtained from  $u = u_1^* + u_2^*$ .

The technique to determine the SIFs is introduced in this section. In Eq. (24), the fundamental solution  $G$  has singularities when  $x_i = s_j$ . Due to the property of the same order of the singularities between the fundamental solutions of Laplace equation [30] and wave equation at the retarded moment  $t_R$ , the SIFs  $Q_i$  at the retarded moment can be expressed as

$$Q_i = Q_i^0 + B, \tag{26}$$

$$Q_i^0 = \frac{\Theta(x_i) - \sum_{j=1, j \neq i}^N G_0(|x_j - x_i|) L_j}{L_i}, \tag{27}$$

where  $\Theta(x_i) = \int_{\Gamma} G_0(|x_i - s|) d\Gamma(s)$  is the integration of the fundamental solution  $G_0$  over the whole physical boundary,  $G_0(|x_i - s|) = \frac{1}{4\pi r(|x_i - s|)}$  the fundamental solution in 3D Laplace equation,  $|x_i - s_j|$  the distance between source point  $s_j$  and collocation point  $x_i$ .  $L_j$  the corresponding range of influence of source points  $s_j$  as shown in Fig. 9,  $Q_i^0$  the SIFs for 3D Laplace equation,  $Q_i$  the SIFs for 3D wave equation at the retarded moment  $t_R$ ,  $B = \frac{ik}{4\pi}$  in 3D wave equation upon Dirichlet boundary condition.

Under the extensive studies, we find that in some specific solid of revolution domain, the  $\Theta(x_i)$  can be calculated directly to avoid the numerical integration. For example, in

sphere-shaped domain, the  $\Theta(x_i)$  can be calculated directly by

$$\Theta(x_i) = \frac{1}{4\pi} \int_0^{2\pi} \int_0^\pi \frac{R^2 \sin(\theta)}{\sqrt{2R^2(1 - \cos\theta)}} d\theta d\phi = R. \tag{28}$$

### 3 Numerical results and discussions

In this section, the accuracy and efficiency of the present SBM are tested to 2D and 3D benchmark examples in comparison with the analytical and linear BEM solutions. The numerical accuracy can be measured by the absolute root mean square errors (Err) and the relative root mean square errors (Rerr) as stated below

$$Err(u) = \sqrt{\frac{1}{NT} \sum_{k=1}^{NT} |u(k) - \bar{u}(k)|^2}, \tag{29a}$$

$$Rerr(u) = \frac{\sqrt{\frac{1}{NT} \sum_{k=1}^{NT} |u(k) - \bar{u}(k)|^2}}{\sqrt{\frac{1}{NT} \sum_{k=1}^{NT} |\bar{u}(k)|^2}}, \tag{29b}$$

where  $\bar{u}(k)$  and  $u(k)$  are the analytical and numerical solutions at  $x_i$ , respectively, and  $NT$  is the total number of the test points in the interest domain  $\Omega$ . To investigate the convergence rate of the present approach in 3D problems, the following formulation is introduced.

$$C_{3D} = -2 \frac{\ln(Error(N_1)) - \ln(Error(N_2))}{\ln(N_1) - \ln(N_2)}, \tag{30}$$

where  $Error(N_1)$  and  $Error(N_2)$  denote the errors  $Rerr(u)$  or  $Err(u)$  of the SBM with  $N_1$  and  $N_2$  source points, respectively. In the direct linear BEM, the discretization formulation introduced in reference [18] is adopted.

#### 3.1 Error analysis

##### 3.1.1 SBM for 2D wave equation

*Example 1* The vibrations of thin membrane in square domain with zero initial conditions.

Consider the unit square domain, namely,  $a = 1, b = 1$ . In this case, the present SBM uses 40 source points ( $N_s = 40$ ) and zero field points ( $N_f = 0$ ), where the distribution of source points is shown in Fig. 10. And the governing equation is given by

$$\begin{cases} u_{tt} = c^2(u_{xx} + u_{yy}), & 0 < x < a, 0 < y < b, t > 0, \\ u|_{t=0} = u_t|_{t=0} = 0, & 0 \leq x \leq a, 0 \leq y \leq b, \\ u|_{x=0} = u|_{x=a} = 0, & 0 \leq y \leq b, t \geq 0, \\ u|_{y=0} = 0, u|_{y=b} = \sin \frac{\pi x}{a} \sin t, & 0 \leq x \leq a, t \geq 0. \end{cases}$$

The analytical solution is given by

$$u(x, y, t) = \frac{y}{a} \sin\left(\frac{\pi x}{a}\right) \sin t + \sum_{m=1}^{\infty} \left( b_{1m} \sin \lambda_{1m} ct + \frac{f_{1m}}{u_{1m}} \sin t \right) \sin\left(\frac{\pi x}{a}\right) \sin\left(\frac{m\pi y}{b}\right),$$

where

$$\lambda_{nm} = \pi \sqrt{\frac{n^2}{a^2} + \frac{m^2}{b^2}},$$

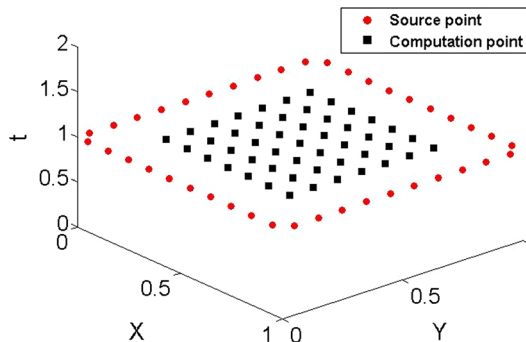
$$f_{1j} = \frac{4}{ab^2} \left( 1 - \frac{c^2 \pi^2}{a^2} \right) \int_0^a \int_0^b y \sin^2 \frac{\pi x}{a} \sin \frac{j\pi y}{b} dx dy$$

$$= \frac{2(-1)^{j+1}}{j\pi} \left( 1 - \frac{c^2 \pi^2}{a^2} \right), \quad j \geq 1$$

$$\mu_{1j} = c^2 \lambda_{1j}^2 - 1 \neq 0,$$

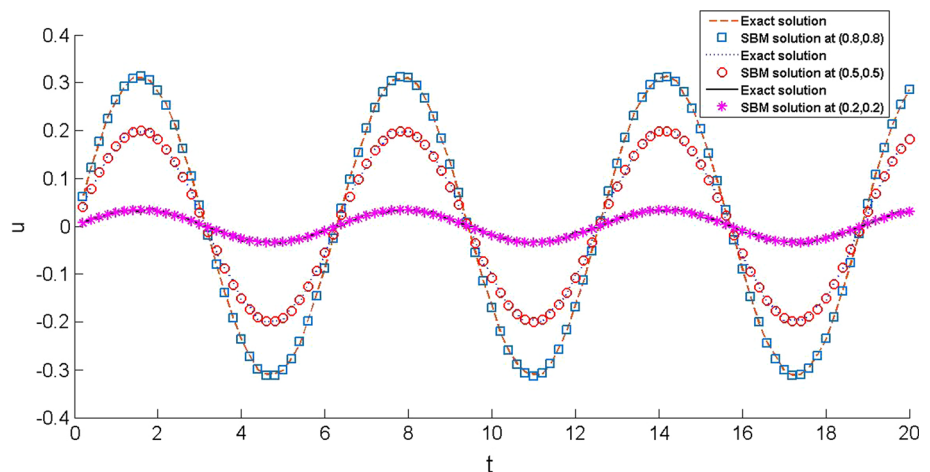
$$b_{1m} = \frac{2(-1)^m}{cm\lambda_{1m}\pi} - \frac{f_{1m}}{c\lambda_{1m}\mu_{1m}}, \quad m \geq 1$$

Figure 11 depicts the displacement history by SBM at (0.8, 0.8), (0.5, 0.5) and (0.2, 0.2) with  $c = 10$ , respec-



**Fig. 10** Distribution of the source and the computation points for 2D membrane vibration problem in a square domain

**Fig. 11** The evolution of numerical results and analytical solutions in square domain



tively. These results agree well with the analytical solution. It shows that the SBM provides the accurate results for two-dimensional membrane vibration problem even using very few source points. Then, Fig. 12 depicts the Maximum absolute errors (Merr) by SBM against time with different velocities ( $c = 10, c = 20$  and  $c = 50$ ), respectively. At last, we list the Table 1 to investigate the numerical accuracy when the test points are close to the boundary and corner with  $c = 10, t = 10, N_s = 40$  and  $N_f = 0$ .

It can be observed that the present SBM has the good performance with different velocities  $c$ . However, the error analysis shows that numerical accuracy has slightly decrease when the test points are close to the boundary and corner.

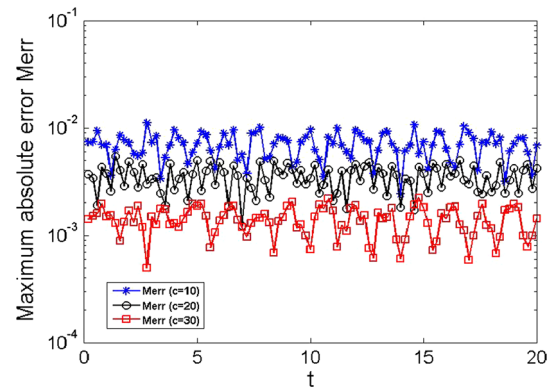


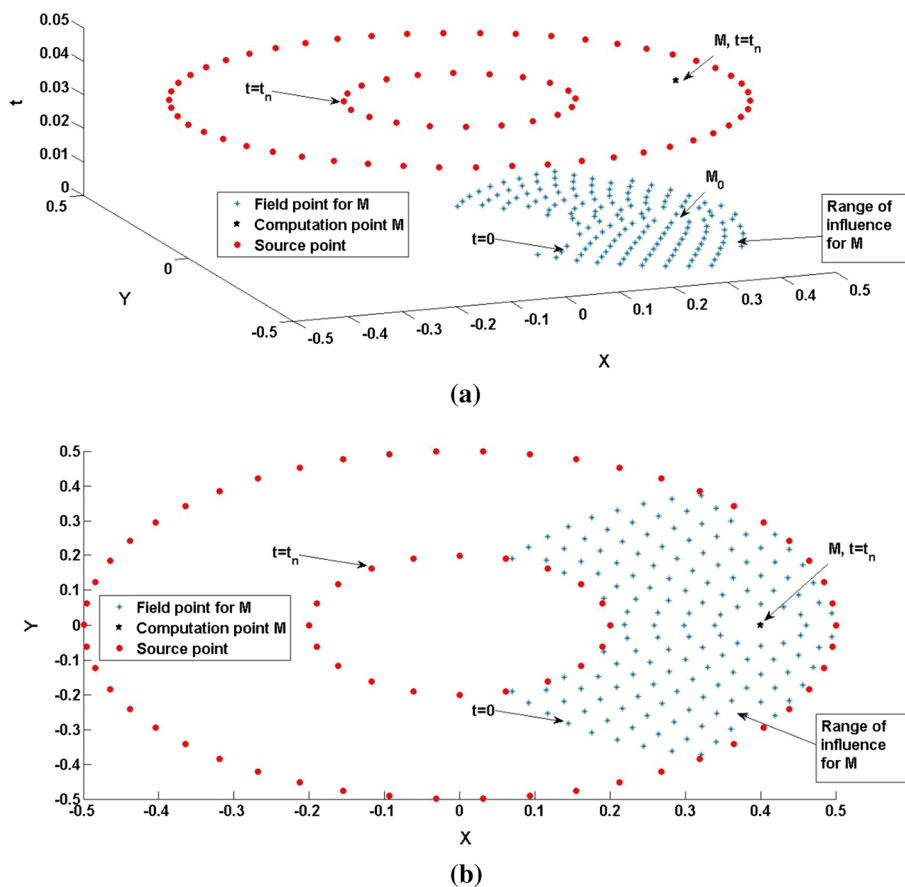
**Fig. 12** The Maximum absolute errors (Merr) by the SBM against time

**Table 1** The numerical results of SBM

Test point	(0.1, 0.1)	(0.1, 0.9)	(0.9, 0.1)	(0.9, 0.9)
Analytical	-4.36E-3	-1.22E-1	-4.36E-3	-1.22E-1
SBM	-4.50E-3	-1.25E-1	-4.50E-3	-1.25E-1
Err	1.43E-4	3.02E-3	1.42E-4	3.00E-3
Rerr	3.28E-2	2.47E-2	3.26E-2	2.46E-2



**Fig. 13** Distribution of the source, field and computation points **a** 3D plot Distribution of the source, field and computation points, **b** 2D contour plot



It is interesting to notice that the SBM can solve this example without using field points due to the initial conditions are zero in this case. Moreover, we only place the source points at one certain time level  $t_n$  as shown in Fig. 2, since 2D kernel function is the fundamental solutions integrating along with time in the present SBM.

*Example 2* The 2D wave propagation in annulus domain with non-zero initial conditions.

Consider the annulus domain with outer radius  $R_2 = 0.5$  and inner radius  $R_1 = 0.2$ . In this case, the present SBM uses 70 source points ( $N_s = 70$ ) and 1255 field points for every computation point ( $N_f = 1255$ ), where the distribution of source points is shown in Fig. 13. And the governing equation is given by

$$\begin{cases} u_{tt} = c^2 (u_{xx} + u_{yy}), & (x, y) \in \Omega \\ u|_{t=0} = 0 \\ u_t|_{t=0} = ck \sin(\frac{k}{\sqrt{2}}(x + y)) \\ \bar{u} = \sin(\frac{k}{\sqrt{2}}(x + y)) \sin(ckt), & (x, y) \in \Gamma \end{cases}$$

In this example, the effect of wave number  $k$  on numerical accuracy is investigated. We fix the velocity  $c = 10$  and choose three different wave numbers ( $k_1 = \frac{\pi}{8}, k_2 = \frac{\pi}{6}$  and

$k_3 = \frac{\pi}{3}$ ). The test points are placed on three circles having radius 0.3, 0.35 and 0.4, respectively. Figure 14 depicts the SBM numerical results in comparison with analytical and linear BEM solutions. It is observed that the SBM solution agree well with the analytical solutions and BEM results with 70 boundary elements.

Figure 15 depicts the Maximum absolute errors (Merr) by SBM against time with different wave numbers ( $k_1 = \frac{\pi}{8}, k_2 = \frac{\pi}{6}$  and  $k_3 = \frac{\pi}{3}$ ). The test points are placed on a circle with radius 0.4.

It can be observed that the present SBM results with different wave numbers are in good agreement with the analytical solutions along with time evolution. And it is worthy of stressing that the SBM only places field points in the corresponding range of influence for every computation point  $M$  in 2D problems as shown in Fig. 13.

### 3.1.2 SBM for 3D wave equation

*Example 3* Wave propagation in a sphere domain.

We first consider a simple case of 3D wave propagation in a sphere domain with radius 1. And the governing equation is given by

**Fig. 14** The numerical results and analytical solutions against angular coordinate  $\theta$  in annulus domain case

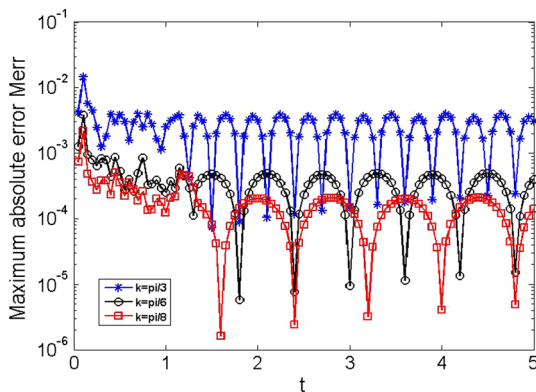
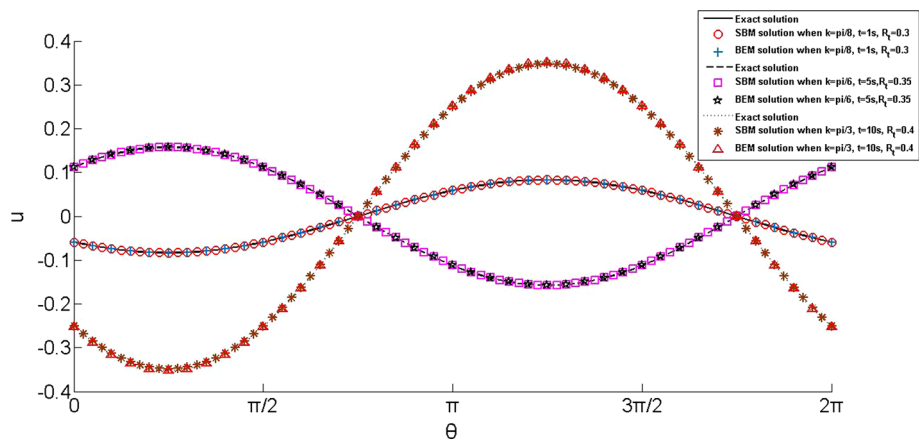


**Fig. 15** The Maximum absolute errors (Merr) by the SBM against time

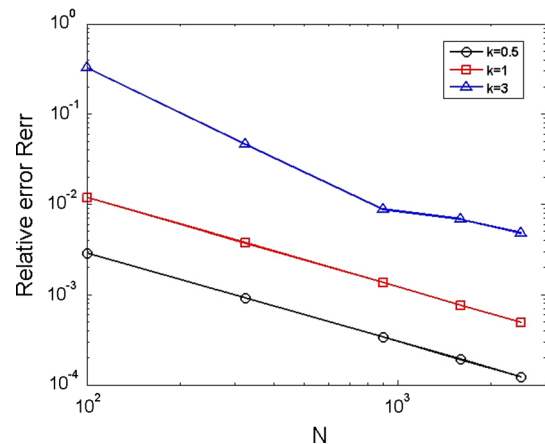


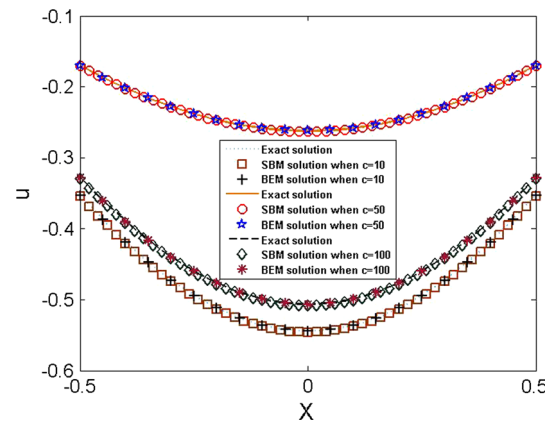
**Fig. 16** The relative root mean square errors (Rerr) by the SBM against source points number  $N_s$

$$\begin{cases} u_{tt} = c^2 (u_{xx} + u_{yy} + u_{zz}), & (x, y, z) \in \Omega \\ u|_{t=0} = 0 \\ u_t|_{t=0} = ck \cos\left(\frac{k}{\sqrt{3}}(x + y + z)\right) \\ \bar{u} = \cos\left(\frac{k}{\sqrt{3}}(x + y + z)\right) \sin(ckt), & (x, y, z) \in \Gamma \end{cases}$$

In this case, the SBM uses time interval  $\Delta t = 2 \times 10^{-1}$  under velocity  $c = 10$  and the field points number  $N_f = 1255$  for every computation point. The test points are placed on a sphere surface with radius 0.5 at  $t = 1s$ . Fig. 16 shows the SBM results against the number of source points under different wave numbers ( $k_1 = 0.5, k_2 = 1$  and  $k_3 = 3$ ). It can be found from Fig. 16 that the SBM converges rapidly to the analytical solution with  $C = 2.0$ . And the more accurate results are obtained with the decreasing wave number.

$$C_{k=0.5} = 2.0, \quad C_{k=1} = 2.0, \quad C_{k=3} = 2.2$$

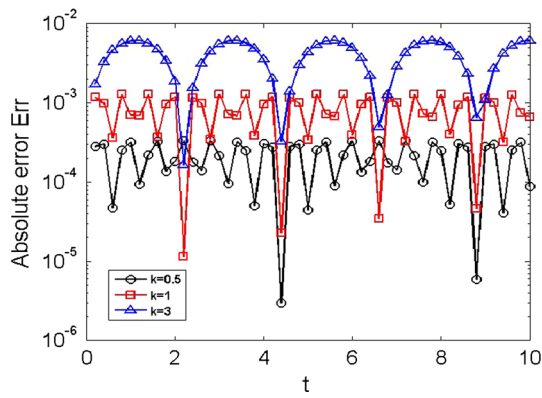
Then, we use time interval  $\Delta t = 2 \times 10^{-1}$  under wave number  $k = 1$  with source points number  $N_s = 324$  and field points number  $N_f = 1255$  for every computation point. The test points are placed on a line  $x = y = z, x \in (-0.5, 0.5)$ .



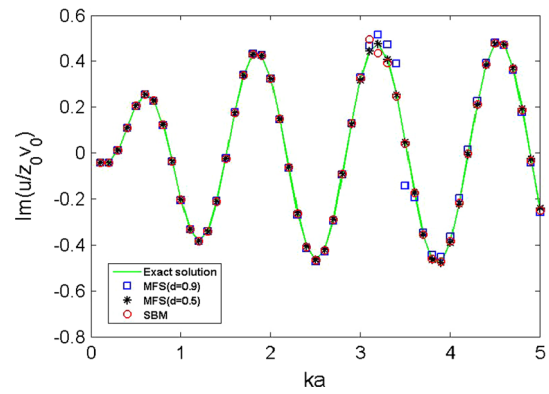
**Fig. 17** The evolution of numerical results and analytical solutions in sphere domain

Figure 17 depicts the SBM numerical results under varied velocity  $c_1 = 10, c_2 = 50$ , and  $c_3 = 100$ , respectively, which match well with the analytical solutions and BEM results with 324 boundary elements.

To further investigate the SBM performance, we use time interval  $\Delta t = 2 \times 10^{-1}$  under velocity  $c = 10$  with source



**Fig. 18** The absolute root mean square errors (Err) by the SBM against time  $t$  in sphere domain



**Fig. 20** Imaginary part of the analytical and numerical solutions

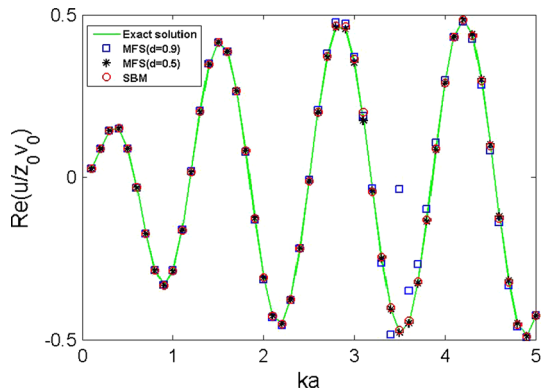


**Fig. 19** Real part of the analytical and numerical solutions

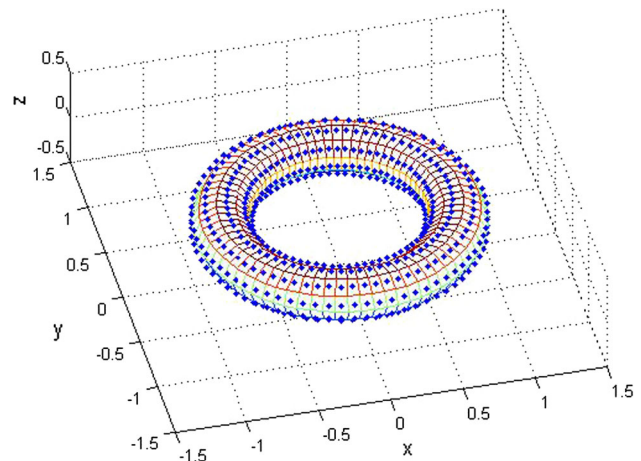


**Fig. 21** The distribution of source points on the tire surface

points number  $N_s = 900$  and field points number  $N_f = 1255$  for every computation point. The test points are placed on a sphere surface of radius 0.5. Fig. 18 shows that the SBM results with respect to time under different wave numbers ( $k_1 = 0.5, k_2 = 1$  and  $k_3 = 3$ ).

*Example 4* Wave propagation for exterior problem.

Consider the acoustic radiation from a pulsating sphere with radius  $a = 1$  and uniform radial velocity  $v_0$ . The analytical solution of the pulsating-sphere model can be represented as [28]

$$u(r, \theta, t) = \frac{a}{r} \left( \frac{ikaz_0}{ika - 1} \right) v_0 e^{ik(r-a) + i\omega t},$$

where  $z_0 = \rho_0 c$  is the characteristic impedance of the medium in which  $\rho_0$  denotes the density of the medium and  $c$  the sound velocity and  $\omega = kc$  the wave frequency.

The Figs. 19 and 20 show the real parts  $\text{Re} \left( \frac{u(2a, 0, 0)}{z_0 v_0} \right)$  and imaginary parts  $\text{Im} \left( \frac{u(2a, 0, 0)}{z_0 v_0} \right)$  of the non-dimensional solution with source points number  $N_s = 400$  and  $\Delta t = 0.5s$ .

It can be observed that the SBM results remain in good agreement with the analytical solutions, except  $ka = \pi$  with slight difference. In addition, the MFS can match well with the analytical solutions when the fictitious boundary  $d = 0.5$ . However, when  $d = 0.9$ , there is considerable error. And it is worthy of stressing that the field point is no longer required in the SBM for this exterior problem.

*Example 5* Wave propagation in a tire-shaped domain.

Consider 3D wave propagation in a tire-shaped domain. The tire surface is defined by the following equation

$$\{(x, y, z) \mid x = (R + r \cos \varphi) \cos \theta, y = (R + r \cos \varphi) \sin \theta, z = r \sin \varphi, 0 \leq \theta, \varphi < 2\pi\},$$

where  $R = 0.8, r = 0.2$ . The distribution of source points on the tire surface is shown in Fig. 21.

And the governing equation is given by

$$\begin{cases} u_{tt} = c^2 (u_{xx} + u_{yy} + u_{zz}), & (x, y, z) \in \Omega \\ u|_{t=0} = 0 \\ u_t|_{t=0} = ck(\cos(kx) + \cos(ky) + \cos(kz)) \\ \bar{u} = (\cos(kx) + \cos(ky) + \cos(kz)) \sin(ckt), & (x, y, z) \in \Gamma \end{cases}$$

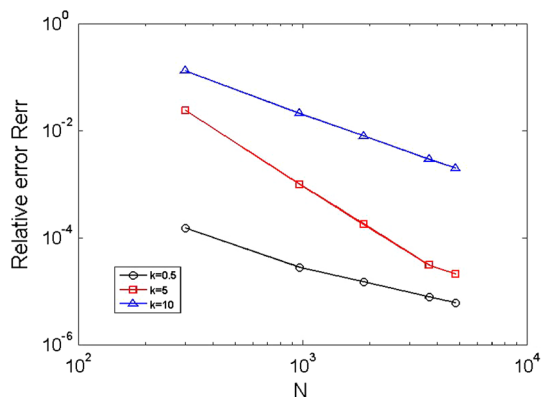


**Fig. 22** The relative root mean square errors (Rerr) by the SBM against source points number  $N_s$

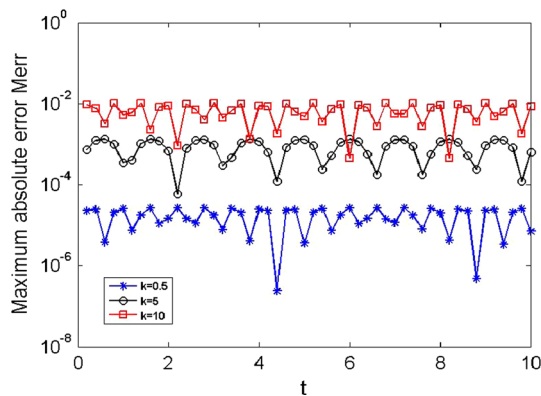


**Fig. 23** The Maximum absolute errors (Merr) by the SBM against time  $t$  in tire-shape domain

In this case, we use time interval  $\Delta t = 2 \times 10^{-1}$  under velocity  $c = 10$  and the field points number  $N_f = 1255$  for every computation point. The test points are placed on a circle having radius 0.8 at  $t = 1s$ . Figure 22 shows the SBM results against the number of source points for Example 5 with different wave numbers ( $k_1 = 0.5$ ,  $k_2 = 5$  and  $k_3 = 10$ ). It can be found from Fig. 22 that the SBM converges rapidly to the analytical solution with  $C = 2.0$ , and the rate of convergence can even reach  $C = 5.0$  when  $k = 5$ .

$$C_{k=0.5} = 2.3, \quad C_{k=5} = 5.0, \quad C_{k=10} = 3.0$$

Then, we use time interval  $\Delta t = 2 \times 10^{-1}$  under velocity  $c = 10$  with source points number  $N_s = 972$  and the field points number  $N_f = 1255$  for every computation point. The test points are placed on a circle with radius 0.8. Figure 23 depicts the SBM results with respect to time at different wave numbers ( $k_1 = 0.5$ ,  $k_2 = 5$  and  $k_3 = 10$ ). It can be observed that as time evolves, the numerical results remain in good agreement with the analytical solutions even in the multi-connected domain.

Through all these 3D benchmark numerical examples, it can be observed that the present SBM results are quite

accurate under different velocities  $c$  and wave numbers  $k$ . And as time evolves, the efficiency and accuracy of the numerical results are still in good agreement with the analytical solutions. The SBM converges remarkably rapidly with the increasing boundary node number  $N_s$ . The error analysis shows that the present SBM has rapid convergence rate ( $C_{3D} = 2$ ) for 3D wave propagation.

## 4 Conclusions

This study makes the first attempt to extend the SBM with time-dependent fundamental solution to two-dimensional and three-dimensional scalar transient wave equation upon Dirichlet boundary condition. In the present SBM, two empirical formulas are proposed to determine the SIFs in 2D and 3D problems, respectively.

In 2D problems, the fundamental solution integrating along with time is applied. The SBM only places the source points at the interested time level  $t_n$ . By introducing the concept of the source intensity factors, there is no numerical integration by the SBM in 2D problems.

In 3D problems, a time-successive evaluation approach based on Huygens principle is proposed, and the time-dependent fundamental solution is applied. There is no complicated mathematical transform by the SBM in 3D problems, and the concept of the field point is introduced.

In this paper, a fundamental difference between the 2D and 3D cases is observed. “The influence due to a source function at the point  $\mathbf{r}$ , on the potential at  $(\mathbf{r}_0, t_0)$  is restricted to the value at the retarded time  $t_R = t_0 - |\mathbf{r} - \mathbf{r}_0|/c$  for the 3D case, whereas, for 2D case, the influence has to be integrated from  $-\infty$  to  $t_R$  [18]”. This difference in response behaviors is because the 2D wave has aftereffect phenomenon, i.e., the dispersion of waves. And in contrast, the 3D wave does not have such an aftereffect phenomenon.

In 2D problems, because the wave has aftereffect phenomenon, the range of influence  $C_{ct_n}^{M_0} \cap \Omega$  will become larger and larger as time evolves. However, it will not be larger than the domain  $\Omega$ . In 3D problems, the wave does not have the aftereffect phenomenon. The field point is no longer required after a certain time, because the range of influence  $S_{ct_n}^M \cap \Omega$  equals zero at that time.

In several benchmark numerical experiments, it can be observed that the present SBM results are quite accurate under different velocities  $c$  and wave numbers  $k$ . As time evolves, the efficiency and accuracy of the numerical results remain in good agreement with the analytical solutions. In 3D wave propagation problems, the SBM converges remarkably quickly with the increasing boundary node number  $N_s$ . The error analysis shows that the present SBM scheme has rapid convergence rate  $C_{3D} = 2$  in all tested 3D examples. Without mesh and complicated mathematical transform, the SBM appears computationally efficient and may be considered a

competitive alternative after further numerical and theoretical study.

It is worth noting that as the first step, we have only considered the 2D and 3D wave equation upon Dirichlet boundary conditions in this study. And the SBM with time-dependent fundamental solutions for scalar wave equation upon Neumann boundary conditions and Robin boundary conditions is under intense study and will be reported in a subsequent paper.

**Acknowledgments** The work described in this paper was supported by the National Science Funds of China (Grant Nos. 11302069, 11372097, 11572111), the Chinese Postdoctoral Science Foundation (Grant Nos.2014M561565, 2015T80492), and the Foundation for Open Project of the State Key Laboratory of Acoustics (Grant No. SKLA201509), the Foundation for Open Project of the key laboratory of road construction technology and equipment, ministry of education (Grant No. 310825151132), the 111 Project (Grant No. B12032).

### Appendix: The detailed derivation of Eq. (13)

The derivation of Eq. (13) will be provided via a circle domain with uniformly distributed points. It is beyond our capability to derive this formula in more general situations. However, our numerical experiments show that Eq. (13) can be extended to irregular domains with non-equally distributed points.

Consider a 2D Laplace equation on Dirichlet boundary condition

$$\nabla^2 u(x) = 0, \quad x \in \Omega, \tag{31}$$

$$u(x) = \bar{u}(x), \quad x \in \Gamma_D, \tag{32}$$

where  $\nabla^2$  denotes the Laplacian operator,  $u(x)$  represents the potentials in domain  $\Omega$ ,  $\bar{u}(x)$  is the known function,  $\Gamma_D$  represents the Dirichlet boundary conditions.

The formulation of the SBM can be stated as

$$\bar{u}(x_m) = \begin{cases} \sum_{n=1}^N \alpha_n G_0(x_m, s_n), & x_m \in \Omega \setminus \partial\Omega \\ \sum_{\substack{n=1 \\ n \neq m}}^N \alpha_n G_0(x_m, s_n) + \alpha_m U_0^m, & x_m \in \Gamma_D \end{cases}, \tag{33}$$

where  $G_0(x_m, s_n) = \ln(r_{mn})$  is the fundamental solution of 2D Laplace equations,  $U_0^m$  the source intensity factors,  $\alpha_n$  the unknown coefficient.

Consider  $\Omega$  a circle with radius  $R$ .  $\{x_m\}_{m=1}^N$  denote the collocation and source points uniformly placed on the boundary  $\partial\Omega$ .  $L_n$  represents the length of the auxiliary line in 2D as shown in Fig. 5.

For  $x_m \in \partial\Omega$ , it is easy to verify that the following contour integral is zero.

$$\oint \ln(r(x_m, s)/R) d\Gamma_s = 0, \tag{34}$$

where  $r$  is the distance between  $x_m$  and source points  $s$  on the circle. Eq. (34) can be discretized as

$$\sum_{n=1}^N \ln(r(x_m, x_n)/R) = 0. \tag{35}$$

Due to the symmetry property of the circle, the derivation is independent of the indices of the collocation points.  $m = 1$  is used in the following derivation. Hence, we have

$$\sum_{n=1}^N \ln(r(x_1, x_n)/R) = 0, \tag{36}$$

where  $x_1 = (1, 0)$ . Notice that

$$r(x_1, x_n) = 2R \sin\left(\frac{n-1}{N}\pi\right). \tag{37}$$

Substituting Eq. (37) into Eq. (36), and define the desingularized value of the natural logarithm function as  $a$ ,

$$a = \ln R - \ln\left(2^{N-1} \prod_{n=2}^N \sin\left(\frac{n-1}{N}\pi\right)\right). \tag{38}$$

The key issue is to determine the value of  $\prod_{n=2}^N \sin\left(\frac{n-1}{N}\pi\right)$ . Let  $\omega = \cos(2\pi/N) + i \sin(2\pi/N) = \exp(2\pi i/N)$ . Note that  $\omega$  is a solution of the equation

$$z^N - 1 = 0. \tag{39}$$

Similarly,  $\omega^2, \omega^3, \dots, \omega^{N-1}$  are also the solution of Eq. (39). After some algebraic manipulations, Eq. (39) is equivalent to

$$z^{N-1} + z^{N-2} + \dots + z + 1 = (z - \omega)(z - \omega^2) \dots (z - \omega^{N-1}), \tag{40}$$

For  $z = 1$ , we obtain

$$N = (1 - \omega)(1 - \omega^2) \dots (1 - \omega^{N-1}). \tag{41}$$

It follows that

$$N = |1 - \omega| |1 - \omega^2| \dots |1 - \omega^{N-1}|. \tag{42}$$

Since

$$1 - \omega^k = 2 \sin \frac{k\pi}{N} \left( \sin \frac{k\pi}{N} - i \cos \frac{k\pi}{N} \right). \tag{43}$$

We have

$$|1 - \omega^k| = 2 \sin \frac{k\pi}{N}. \tag{44}$$



Therefore,

$$\prod_{n=2}^N \sin\left(\frac{n-1}{N}\pi\right) = \frac{N}{2^{N-1}}. \quad (45)$$

From Eqs. (38) and (45), we have

$$a = \ln(R/N). \quad (46)$$

It follows that  $U_0^m$  for the natural logarithm function is

$$U_0^m = \ln\left(\frac{2\pi R}{2\pi N}\right) = \ln\left(\frac{L_m}{2\pi}\right), \quad (47)$$

where  $L_m = 2\pi R/N$ .

## References

- Young DL, Gu MH, Fan CM (2009) The time-marching method of fundamental solutions for wave equations. *Eng Anal Bound Elem* 33:1411–1425. doi:10.1016/j.enganabound.2009.05.008
- Chen KH, Chen JT, Chou CR, Yueh CY (2002) Dual boundary element analysis of oblique incident wave passing a thin submerged breakwater. *Eng Anal Bound Elem* 26:917–928. doi:10.1016/S0955-7997(02)00035-8
- Šarler B (2009) Solution of potential flow problems by the modified method of fundamental solutions: Formulations with the single layer and the double layer fundamental solutions. *Eng Anal Bound Elem* 33:1374–1382. doi:10.1016/j.enganabound.2009.06.008
- Zienkiewicz OC, Taylor RL (1991) *The finite element method*, 4th edn. McGraw-Hill, New York
- Avilez-Valente P, Seabra-Santos FJ (2004) A Petrov–Galerkin finite element scheme for the regularized long wave equation. *Comput Mech* 34:256–270. doi:10.1007/s00466-004-0570-4
- He ZC, Liu GR, Zhong ZH, Zhang GY, Cheng AG (2010) Dispersion free analysis of acoustic problems using the alpha finite element method. *Comput Mech* 46:867–881. doi:10.1007/s00466-010-0516-y
- Chen KH, Chen JT (2006) Adaptive dual boundary element method for solving oblique incident wave passing a submerged breakwater. *Comput Method Appl Mech* 196:551–565. doi:10.1016/j.cma.2006.06.002
- Cheng AHD, Cheng DT (2005) Heritage and early history of the boundary element method. *Eng Anal Bound Elem* 29:268–302. doi:10.1016/j.enganabound.2004.12.001
- Carrer JAM, Mansur WJ, Vanzuit RJ (2009) Scalar wave equation by the boundary element method: a D-bem approach with non-homogeneous initial conditions. *Comput Mech* 44:31–44. doi:10.1007/s00466-008-0353-4
- Chen CS, Karageorghis A, Smyrlis YS (2008) *The method of fundamental solutions—a meshless method*. Dynamic Publishers, Atlanta
- Gu MH, Young DL, Fan CM (2009) The method of fundamental solutions for one-dimensional wave equations. *Comput Mater Contin* 11:185–208. doi:10.3970/cmcc.2009.011.185
- Chen CS, Fan CM, Monroe J (2008) The method of fundamental solutions for solving elliptic partial differential equations with variable coefficients. In: Chen CS, Karageorghis A, Smyrlis YS (eds) *The method of fundamental solutions—a meshless method*. Dynamic Publishers Inc, Atlanta, pp 105–175
- Tan SR, Huang LJ (2014) An efficient finite-difference method with high-order accuracy in both time and space domains for modelling scalar-wave propagation. *Geophys J Int* 197:1250–1267. doi:10.1093/gji/ggu077
- Chen HM, Zhou H, Zhang QC, Xia MM, Li QQ (2016) A k-space operator-based least-squares staggered-grid finite-difference method for modeling scalar wave propagation. *Geophysics* 81:T39–T55. doi:10.1190/geo2015-0090.1
- Kim J, Kim D, Choi H (2001) An immersed-boundary finite-volume method for simulations of flow in complex geometries. *J Comput Phys* 171:132–150. doi:10.1006/jcph.2001.6778
- Anastasiou K, Chan CT (1997) Solution of the 2D shallow water equations using the finite volume method on unstructured triangular meshes. *Int J Numer Meth Fluids* 24:1225–1245. doi:10.1002/(SICI)1097-0363(19970615)24:11<1225:AID-FLD540>3.0.CO;2-D
- Rabczuk T, Belytschko T (2004) Cracking particles: a simplified meshfree method for arbitrary evolving cracks. *Int J Numer Methods Eng* 61:2316–2343. doi:10.1002/nme.1151
- Nguyen VP, Rabczuk T, Bordas S, Duflot M (2008) Meshless methods: a review and computer implementation aspects. *Math Comput Simul* 79:763–813. doi:10.1016/j.matcom.2008.01.003
- Fu ZJ, Chen W, Yang W (2009) Winkler plate bending problems by a truly boundary-only boundary particle method. *Comput Mech* 44:757–763. doi:10.1007/s00466-009-0411-6
- Chen W, Wang FZ (2010) A method of fundamental solutions without fictitious boundary. *Eng Anal Bound Elem* 34:530–532. doi:10.1016/j.enganabound.2009.12.002
- Xu SZ (1995) *The boundary element method in geophysics*. Science Press, Beijing
- Brebbia CA (1981) *Progress in boundary element methods*, vol 2. Springer, New York
- Cheng AHD, Young DL, Tsai CC (2000) Solution of poisson's equation by iterative DRBEM using compactly supported, positive definite radial basis function. *Eng Anal Bound Elem* 24:549–557. doi:10.1016/S0955-7997(00)00035-7
- Li JP, Chen W, Fu ZJ (2016) Numerical investigation on convergence rate of singular boundary method. *Math Probl Eng* 2016:1–13. doi:10.1155/2016/3564632
- Wei X, Chen W, Sun LL, Chen B (2015) A simple accurate formula evaluating origin intensity factor in singular boundary method for two-dimensional potential problems with Dirichlet boundary. *Eng Anal Bound Elem* 58:151–165. doi:10.1016/j.enganabound.2015.04.010
- Sun LL, Chen W, Cheng AHD (2016) Singular boundary method for 2D dynamic poroelastic problems. *Wave Motion* 61:40–62. doi:10.1016/j.wavemoti.2015.10.004
- Chen W, Zhang JY, Fu ZJ (2014) Singular boundary method for modified Helmholtz equations. *Eng Anal Bound Elem* 44:112–119. doi:10.1016/j.enganabound.2014.02.007
- Fu ZJ, Chen W, Chen JT, Qu WZ (2014) Singular boundary method: three regularization approaches and exterior wave applications. *CMES-Comput Model Eng* 99:417–443. doi:10.3970/cmcs.2014.099.255
- Li JP, Fu ZJ, Chen W (2016) Numerical investigation on the obliquely incident water wave passing through the submerged breakwater by singular boundary method. *Comput Math Appl* 71:381–390. doi:10.1016/j.camwa.2015.11.025
- Fu ZJ, Chen W, Gu Y (2014) Burton–Miller-type singular boundary method for acoustic radiation and scattering. *J Sound Vib* 333:3776–3793. doi:10.1016/j.jsv.2014.04.025